Ultra-short plasmonic polarization beam splitter-rotator using a bent directional coupler

Bing Bai (白 冰), Li Pei (裴 丽)*, Jingjing Zheng (郑晶晶), Tigang Ning (宁提纲), and Jing Li (李 晶)

Key Laboratory of All Optical Network and Advanced Telecommunication Network, Ministry of Education, Institute of Lightwave Technology, Beijing Jiaotong University, Beijing 100044, China

**Corresponding author: lipei@bjtu.edu.cn*

Received September 15, 2019; accepted December 26, 2019; posted online April 1, 2020

We propose and analyze a silicon hybrid plasmonic polarization splitter-rotator with an ultra-short footprint using an asymmetric bent directional coupler on a silicon-on-insulator platform. Benefitting from the large birefringence induced by the bent structure and plasmonic effect, the cross-polarization coupling length is only 5.21 μm. The transverse magnetic to transverse electric polarization conversion efficiency is over 99.9%, with an extinction ratio of 20.6 dB (32.5 dB) for the transverse magnetic (transverse electric) mode at 1.55 μm. Furthermore, the polarization conversion efficiency is higher than 90% while maintaining cross talk below −19 dB within the bandwidth of 80 nm.

Keywords: polarization sensitive devices; surface plasmons; integrated optics devices.
doi: 10.3788/COL202018.041301.

Silicon-on-insulator (SOI) platforms have recently attracted a great amount of attention for photonic integration due to the compactness and compatibility with the mature CMOS fabrication process. The high index contrast between Si and SiO_2 enables dense photonic integration. However, high polarization dependence also emerges. One common approach to handling this problem is applying an on-chip polarization diversity scheme[1] to eliminate the polarization sensitivity. The polarization beam splitter-rotator (PSR) is a basic functional element that allows for simultaneous polarization splitting and rotating of light beams. Until now, different designs for PSRs have been reported, including the asymmetric directional coupler (DC)[2–12], multimode interference (MMI)[13,14], adiabatic tapers[14–18], subwavelength grating (SWG)[19–22], and so on. Table 1 shows a comparison of the reported polarization beam splitter-rotators when the coupling length (L_c) < 20 μm.

Normally straight waveguides are exploited in these structures due to their relatively easy design rules. There are two types of PSRs, in principle. One is based on hybridized mode evolution and the other is hybridized cross-polarization coupling. The PSRs utilizing mode evolution tapers require a long device length to transform the fundamental transverse magnetic (TM) mode to the first higher-order transverse electric (TE_1) mode with high efficiency. The TE_1 mode then converts to the fundamental transverse electric (TE) mode via MMI[13,14], a Mach–Zehnder interferometer (MZI)[15], Y junction[16], or asymmetric DC[17,23]. For mode coupling ones, if two orthogonal modes (TE and TM) have equal propagation constants, and the vertical or horizontal symmetry is broken, cross-polarization coupling will occur. Liu *et al.*[6] demonstrated a PSR by using two parallel waveguides and an extinction ratio (ER) >12 dB with an L_c of 36.8 μm obtained experimentally within the C-band. Wang *et al.*[4] proposed a PSR based on a rib asymmetrical directional coupler with $L_c = 24$ μm and ER = 12 dB. To broaden the fabrication tolerance, a tapered DC[24,25] and SWG[20,21,19] are applied with $L_c > 20$ μm. PSRs using a bent DC have been proposed[10] and experimentally achieved[11,12]. These devices are compact due to the relatively strong birefringence of the SOI platform. However, it is challenging to further shrink the footprint of these devices because of the birefringence limitation of the silicon waveguide. New materials and structures should be introduced to effectively reduce the dimensions of the PSRs.

Thanks to the natural polarization sensitivity and subwavelength optical waveguiding[26], the hybrid plasmonic waveguide (HPW)[27] is a promising candidate for on-chip polarization control. PSRs utilizing asymmetrical plasmonics-assisted directional coupling[8,9] have been theoretically investigated, while the L_c (11.2 μm[8] and 7.7 μm[9]) is still relatively large. Consequently, ultracompact schemes for PSRs with a reasonable performance are still needed.

In this Letter, we propose an ultra-short and highly efficient plasmonic PSR based on a bent DC. The widths of the two bent waveguides are carefully chosen to satisfy the phase-matching condition. Efficient TM–TE cross-polarization occurs between the parallel silicon waveguide and hybrid plasmonic waveguide. Due to the bent structure and plasmonics-induced asymmetry, birefringence is greatly enhanced, which results in an ultracompact L_c of only 5.21 μm. The total length of the device is about 11.2 μm, including the coupling length (L_c) and the input/output sections ($L_{in} + L_o$). It could be further reduced by shortening the taper length. Compared with other PSRs (Table 1), this PSR achieves a record shortest coupling length, to the best of our knowledge. At 1.55 μm,

 © 2020 Chinese Optics Letters

Table 1. Summary of Compact Polarization Beam Splitter-Rotators

Reference No. (*: Experiment)	Coupling Length/μm	ER/dB	IL/dB
[7]	17.4	18	0.22
[8]	11.2	30	0.42
[9]	7.7	50.9	1.545
*[11]	15.7	18	0.4
*[12]	8.8	27	0.135
[22]	8.2	34.7	0.12
This work	5.21	20.6	3.2

TM–TE polarization conversion efficiency (PCE) is over 99.9%, with ER = 20.6 dB (32.5 dB) for TM (TE) polarization. The insertion loss (IL) for the TE (TM) mode is around 0.08 dB (3.22 dB).

Figure 1 shows the proposed PSR designed on a SOI wafer with a 220 nm thick (H) Si layer. The cross-polarization coupling region consists of a bent silicon HPW and a bent strip dielectric waveguide (DW) with $L_c = 5.21$ μm. The metal material is Ag with a height of $h_m = 100$ nm. The thin low-index layer in the HPW is Si_3N_4. The gap between the two waveguides G is set to 150 nm, which is large enough to simplify the fabrication. To break the vertical symmetry, air is adopted as the top cladding. The wavelength λ is 1.55 μm, and the corresponding refractive indices for Ag, SiO_2, Si_3N_4, and Si are $0.143 + 11.364i$[28], 1.444, 1.99, and 3.478, respectively.

The widths of the two bent waveguides (W_m and W_d) are carefully chosen to satisfy the phase-matching condition[29]: equal optical path lengths (OPLs). Thus,

$$\mathrm{OPL} = P\theta = N_d k_0 R_d \theta = N_m k_0 R_m \theta, \tag{1}$$

where P is the propagation constant in a cylindrical coordinate system, θ is the arc-angle for the bent coupling region, $k_0 = 2\pi/\lambda$ is the wavenumber in vacuum. N_d and N_m represent the effective indices of the fundamental TM mode and TE mode supported by the DW and HPW, respectively, and R_d and R_m are the corresponding bending radii. The DW is chosen as the inner bend because the TE mode is naturally better confined in the inner bend while the TM mode is relatively easier coupling to the TE mode in the outer bent HPW. From Fig. 1, the relation between R_d and R_m is $R_m = R_d + W_d/2 + G + W_m/2 = R + G/2 + W_m/2$. Here, R is the equivalent radius of the coupling region and R_m is 10 μm as a tradeoff between low bending losses for both polarizations and the increasing phase mismatch for the non-coupled polarization.

The propagation constants of the two waveguides (Fig. 2) are calculated separately by using the finite element method (FEM). From Eq. (1), we can see that not only the effective indices but also the bending radii influence the phase-match condition. For the DW, the small refractive index and bending radius of the TM mode enlarge the width difference of the two waveguides, which means the birefringence is greatly enhanced. The widths are optimized to be $W_m = 305$ nm and $W_d = 595$ nm (circles in Fig. 2) to have an equal propagation constant of 64 rad. In this instance, efficient TM–TE cross-polarization coupling occurs, while the cross talk is effectively inhibited. Due to the unique plasmonics-assisted double-bend structure, the footprint can be ultrashort and the ER shall be high.

The coupling coefficient $\kappa_{\sigma\tau}$ in the cylindrical coordinate system can be written as

$$\kappa_{\sigma\tau} = \omega \int_0^{+\infty} \int_0^{2\pi} \Delta\varepsilon \overrightarrow{E_\sigma^*} \cdot \overrightarrow{E_\tau} r \mathrm{d}r \mathrm{d}\phi, \tag{2}$$

according to the coupled-mode theory[30]. Here, ω is the frequency, $\Delta\varepsilon$ is the dielectric constant perturbation, and E_σ and E_τ are electric field distributions of the TE mode in the HPW and the TM mode in the DW, respectively. Then, the coupling length $L_c = \pi/(2|\kappa_{\sigma\tau}|)$. In the HPW, the TE mode comprises the photonic TE mode (parallel electric field component) and the SPP mode (vertical electric field component). The proportion of the SPP component depends on the distance between the metal layer and the silicon waveguide[31]. Specifically, the smaller the Si_3N_4

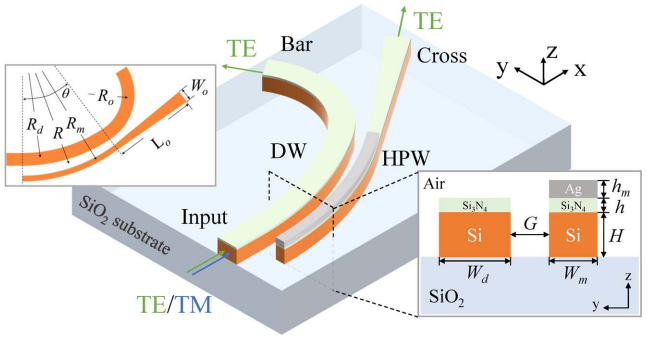

Fig. 1. Schematic layout of the proposed PSR based on a plasmonics-assisted bent directional coupler. Inset: top view and cross section of the coupling region.

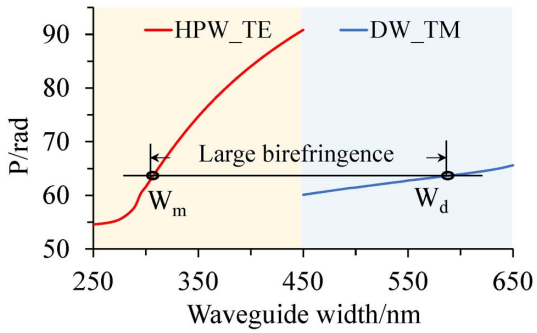

Fig. 2. Propagation constant (P) in cylindrical coordinates for the TE and TM modes in the HPW and the DW versus the waveguide width.

spacer layer thickness h, the more the vertical electric field component in the HPW will be[9]. In the DW, the major electric field component of the TM mode is perpendicular to the interface. Since κ is proportional to the amount of the parallel component between the two optical modes, it can be greatly enlarged by reducing h. However, the propagation loss will rise dramatically if choosing a thin spacer layer. Here, we set $h = 10$ nm as a compromise.

The normalized electric field distributions of supermodes in the coupling region are illustrated in Fig. 3. For cross-polarization coupling, assuming the two supermodes [Figs. 3(a) and 3(b)] have different propagation constants P_1 and P_2, the power of the light exchange between the two waveguides can be regarded as their beating. The power coupled to the cross waveguide reaches the maximum value when $L_c = R\pi/(|P_1 - P_2|)$. Due to the large phase mismatch induced by the bent structure and the plasmonic effect, the coupling under the same polarization state can hardly occur between the two waveguides [Figs. 3(c) and 3(d)].

The propagation of the optical field in the proposed PSR is simulated by the 3D FEM. The minimum mesh cell is $\Delta x \cdot \Delta y \cdot \Delta z = 30$ nm $\times$ 30 nm $\times$ 2 nm, which is small enough to achieve accurate and stable results. The power distributions for the TE and TM mode inputs are shown in Fig. 4. When the TM mode is launched into the DW, the optical signal is coupled and simultaneously converted to the TE mode in the HPW, then gradually transfers the hybrid plasmonic TE mode into the traditional photonic TE mode via the taper, and exits from the Cross port. The insets show the hybridization process in the coupling region at the corresponding positions [Fig. 4(a)]. For the TE mode input, the optical signal just passes through the waveguide with almost no coupling [Fig. 4(b)] due to the large phase mismatch induced by the plasmonics and bent structure. Therefore, the input TM mode is separated from the TE mode and simultaneously rotated by the bent directional coupler over a short length. The small bend ($R_0 = 3$ μm) at the Bar port is designed to filter the unwanted TM mode with negligible loss for TE polarization. The taper attached to the HPW is

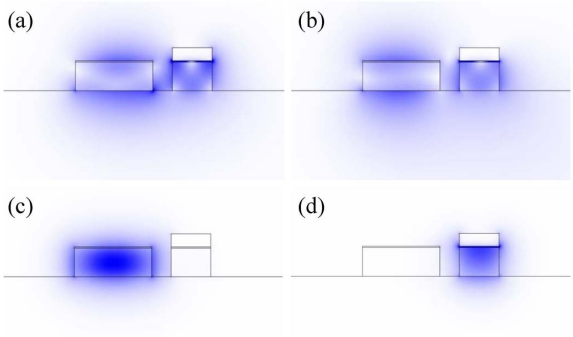

Fig. 3. Normalized electric field distributions of supermodes at (a), (b) efficient cross-polarization coupling and weak (c) TE and (d) TM coupling conditions. Here, $W_m = 305$ nm, $W_d = 595$ nm, and $G = 150$ nm.

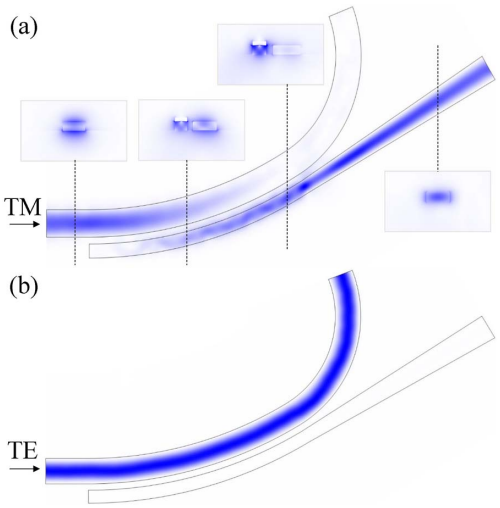

Fig. 4. Power distributions for (a) TM-polarized and (b) TE-polarized light inputs. The insets in (a) show the electric field distributions at the corresponding positions (black dashed lines). Here, $G = 150$ nm, $W_m = 305$ nm, $W_d = 595$ nm, $R_m = 10$ μm, and $L_c = 5.21$ μm.

$L_o = 5$ μm in length, and its width varies from 305 nm to 595 nm. The taper enables the device to conveniently cascade with other optical components.

Polarization conversion efficiency (PCE) is a key figure of merit for a PSR, given by[32]

$$\mathrm{PCE} = 10\log[T_{\mathrm{Cross\_TE}}/(T_{\mathrm{Cross\_TE}} + T_{\mathrm{Bar\_TM}})], \quad (3)$$

where $T_{\mathrm{Cross\_TE}}$ and $T_{\mathrm{Bar\_TM}}$ are the transmissions of the TE and TM modes when the TM mode is injected at the input port. Another is the extinction ratio (ER), defined as

$$\begin{aligned} \mathrm{ER_{TM}} &= 10\log(T_{\mathrm{Cross\_TE}}/T_{\mathrm{Cross\_TM}}), \\ \mathrm{ER_{TE}} &= 10\log(T_{\mathrm{Bar\_TE}}/T_{\mathrm{Bar\_TM}}), \end{aligned} \quad (4)$$

where $T_{\mathrm{Cross\_TM}}$ is the TM mode transmission at the Cross port under the TM mode incidence. $T_{\mathrm{Bar\_TE}}$ and $T_{\mathrm{Bar\_TM}}$ [in Eq. (4)] are the TE and TM mode transmissions at the Bar port under the TE mode incidence. The other important parameters are insertion loss (IL) and cross talk (CL), written as

$$\begin{aligned} \mathrm{IL_{TM}} &= -10\log(T_{\mathrm{Cross\_TE}}), \\ \mathrm{IL_{TE}} &= -10\log(T_{\mathrm{Bar\_TE}}), \end{aligned} \quad (5)$$

$$\begin{aligned} \mathrm{CL_{TE}} &= 10\log(T_{\mathrm{Thru\_TE}}/T_{\mathrm{Cross\_TE}}), \\ \mathrm{CL_{TM}} &= 10\log(T_{\mathrm{Cross\_TE}}/T_{\mathrm{Thru\_TE}}). \end{aligned} \quad (6)$$

For the TM mode incidence, the transmissions are wavelength dependent and $T_{\mathrm{Cross\_TM}}$ reaches its minimum value at the desired wavelength of 1.55 μm [Fig. 5(a)]. $\mathrm{ER_{TM}} > 15$ dB and $\mathrm{IL_{TM}} < 5$ dB are achieved within the wavelength range of 1.5 μm to 1.56 μm. At 1.55 μm, $\mathrm{ER_{TM}}$ is 20.6 dB with a bit higher $\mathrm{IL_{TM}}$ of

3.22 dB compared with other work[8]. The loss comes from three aspects: one is the absorption loss of the metal material; another is the bending loss of the bent directional coupler; the third one is the coupling loss from hybrid plasmonic mode to the dielectric photonic mode at the interface between the HPW and the taper. The absorption loss of the HPW rises as the spacer layer thickness h decreases[33]. Therefore, the propagation loss could be reduced by increasing the spacer layer thickness. The bending loss can be easily suppressed when choosing a larger bending radius. The scattering loss mainly arises from the optical field distribution mismatch between the hybrid plasmonic mode and photonic mode. By adding a plasmonic tapered mode converter between the HPW and the SOI waveguide, the scattering loss could be effectively reduced.

For the TE mode input [Fig. 5(b)], the transmissions are not sensitive to wavelength variation in the range of 1.5 μm to 1.56 μm. ER_{TE} is above 32 dB and the IL_{TE} is better than 0.08 dB within this range due to the large phase mismatch. For the wavelengths less than 1.5 μm, the effective index, i.e., the propagation constant of the TE mode in the HPW increases significantly, which reduces the phase mismatch. Therefore, IL_{TE} rises as the wavelength declines due to the part of light coupled to the HPW. At 1.55 μm, the TM–TE PCE is over 99.9% with a CL less than −23 dB and −33 dB for TM and TE incidence, respectively (Fig. 6). Furthermore, the PCE is higher than 90% while maintaining CL below −19 dB within the bandwidth of 80 nm. Within the wavelength range of 1.45 μm to 1.5 μm, CL increases as the wavelength drops for both polarizations because of the decreasing phase mismatch. Since the refractive indices used in the theoretical calculation are directly from experimental data, there are some fluctuations in the curves (Figs. 5 and 6).

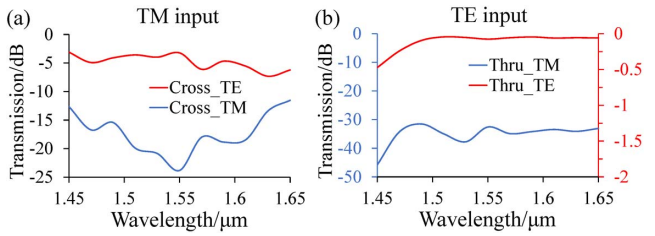

Fig. 5. Wavelength dependence of the PSR. The transmission spectral responses for (a) TM and (b) TE mode input.

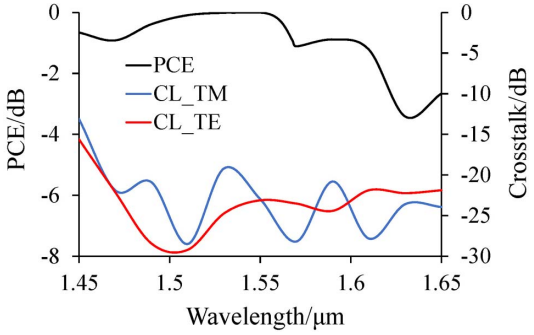

Fig. 6. PCE and CL of the PSR as a function of wavelength.

We further investigate the fabrication tolerance of the proposed PSR. According to the linewidth uniformity of the CMOS technology[28], the two adjacent bent waveguides in the coupling region have the same width variance ΔW. Therefore, the two waveguide widths and coupling gap should be $W'_m = W_m + \Delta W$, $W'_d = W_d + \Delta W$, and $G' = G - \Delta W$. Here, ΔW is the waveguide width deviation. When the TE-polarized light is launched [Fig. 7(a)], the transmissions are slightly affected by ΔW. Although ER_{TE} drops and IL_{TE} rises as ΔW increases due to the decreasing phase mismatch, ER_{TE} is over 30 dB while IL_{TE} is below 0.14 dB in the wide range of $-30\ \text{nm} \le \Delta W \le 30\ \text{nm}$. For TM mode incidence [Fig. 7(b)], however, the transmissions are strongly dependent on ΔW because the propagation constant of the TE mode in the HPW is very sensitive to the waveguide width. $ER_{TM} > 10$ dB and $IL_{TM} < 5.75$ dB are obtained in the range of $-8\ \text{nm} \le \Delta W \le 11\ \text{nm}$. The PCE is over 91% when $-4\ \text{nm} \le \Delta W \le 6\ \text{nm}$. Although ΔW has a significant impact on the phase-match condition, such fabrication accuracy can be guaranteed if using the electron beam lithography (EBL) technique. The phase-matching condition is also dependent on the thickness of the Si_3N_4 layer h, especially for TM mode incidence [Fig. 7(d)]. $ER_{TM} > 10$ dB and $IL_{TM} < 5.3$ dB are realized when $-3\ \text{nm} \le \Delta h \le 5\ \text{nm}$. Fortunately, h can be precisely controlled by optimizing the fabrication process. In the actual fabrication process of Si_3N_4 film prepared by PECVD, the depositing speed, depositing time, gas pressure, and temperature should be optimized in order to precisely control the Si_3N_4 layer thickness and the uniformity. Profiler and scanning electron microscopes can also be used to check the surface flatness. For TE polarization, however, the influence is slight [Fig. 7(c)]. ER_{TE} is higher than 29 dB with IL_{TE} less than 0.08 dB in the range of $-5\ \text{nm} \le \Delta h \le 5\ \text{nm}$.

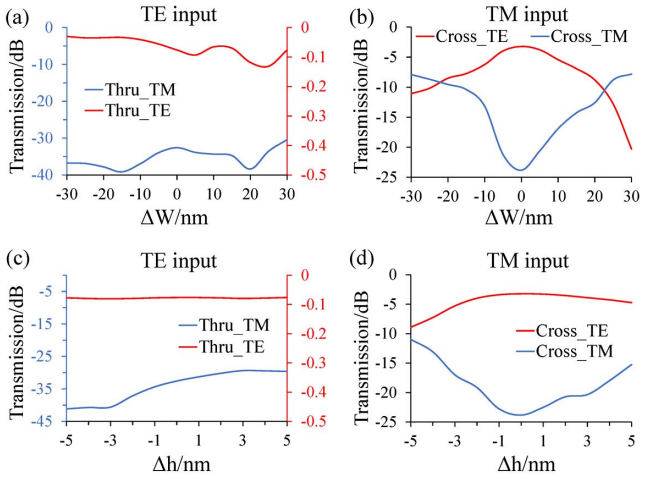

Fig. 7. Transmissions as functions of (a), (b) ΔW and (c), (d) Δh, for TM and TE mode incidence.

In summary, a plasmonic polarization beam splitter-rotator based on an asymmetrical bent directional coupler is proposed. Benefitting from the bent structure and plasmonics-assisted asymmetry, birefringence is greatly enhanced, which results in an efficient cross-polarization coupling in a record shortest distance of only 5.21 μm. At 1.55 μm, a high polarization conversion efficiency $> 99.9\%$ is achieved with $\mathrm{ER_{TM}} = 20.6$ dB and $\mathrm{IL_{TM}} = 3.22$ dB. In addition, a polarization conversion efficiency higher than 90% with cross talk below −19 dB is obtained within the bandwidth of 80 nm. Furthermore, the proposed structure can be flexibly integrated with other photonic devices on SOI platforms and it provides a potential solution for future polarization-insensitive, high-density photonic integrated circuits.

This work was partially supported by the National Natural Science Foundation of China (NSFC) (Nos. 61827817 and 61525501).

References

1. T. Barwicz, M. R. Watts, M. A. Popović, P. T. Rakich, L. Socci, F. X. Kärtner, E. P. Ippen, and H. I. Smith, Nat. Photonics **1**, 57 (2007).
2. L. Socci, V. Sorianello, and M. Romagnoli, Opt. Express **23**, 19261 (2015).
3. H. Guan, A. Novack, M. Streshinsky, R. Shi, Q. Fang, A. E. Lim, G. Lo, T. Baehr-Jones, and M. Hochberg, Opt. Express **22**, 2489 (2014).
4. J. Wang, B. Niu, Z. Sheng, A. Wu, X. Wang, S. Zou, M. Qi, and F. Gan, Opt. Express **22**, 4137 (2014).
5. H. Guan, Q. Fang, G. Q. Lo, and K. Bergman, IEEE Photonics Technol. Lett. **27**, 518 (2015).
6. L. Liu, Y. Ding, K. Yvind, and J. M. Hvam, Opt. Express **19**, 12646 (2011).
7. Y. Fei, L. Zhang, T. Cao, Y. Cao, and S. Chen, Appl. Opt. **51**, 8257 (2012).
8. M. Yin, Q. Deng, Y. Li, X. Wang, and H. Li, IEEE Photonics Technol. Lett. **27**, 229 (2015).
9. B. Bai, L. Liu, and Z. Zhou, Opt. Lett. **42**, 4752 (2017).
10. K. Tan, Y. Huang, G. Lo, C. Lee, and C. Yu, Opt. Express **24**, 14506 (2016).
11. K. Tan, Y. Huang, G. Lo, C. Yu, and C. Lee, Opt. Express **25**, 3234 (2017).
12. Y. Zhang, Y. He, X. Jiang, B. Liu, C. Qiu, Y. Su, and R. A. Soref, APL Photonics **1**, 91304 (2016).
13. Y. Ding, H. Ou, and C. Peucheret, Opt. Lett. **38**, 1227 (2013).
14. J. Wang, M. Qi, Y. Xuan, H. Huang, Y. Li, M. Li, X. Chen, Q. Jia, Z. Sheng, A. Wu, W. Li, X. Wang, S. Zou, and F. Gan, Opt. Express **22**, 27869 (2014).
15. H. Guan, A. Novack, M. Streshinsky, R. Shi, Y. Liu, Q. Fang, A. E. Lim, G. Lo, T. Baehr-Jones, and M. Hochberg, IEEE Photonics Technol. Lett. **26**, 925 (2014).
16. J. Wang, B. Niu, Z. Sheng, A. Wu, W. Li, X. Wang, S. Zou, M. Qi, and F. Gan, Opt. Express **22**, 13565 (2014).
17. D. Dai and J. E. Bowers, Opt. Express **19**, 10940 (2011).
18. D. Chen, X. Xiao, L. Wang, W. Liu, and Q. Yang, Chin. Opt. Lett. **14**, 041301 (2016).
19. Y. Xiong, J. G. Wangüemert-pérez, D. Xu, J. H. Schmid, P. Cheben, and W. N. Ye, Opt. Lett. **39**, 6931 (2014).
20. T. Hu, M. S. D. Rouifed, H. Qiu, X. Guo, C. G. Littlejohns, C. Liu, and H. Wang, IEEE Photonics Technol. Lett. **28**, 911 (2016).
21. Y. Wang, M. Ma, H. Yun, Z. Lu, X. Wang, N. A. F. Jaeger, and L. Chrostowski, IEEE Photonics J. **8**, 7505709 (2016).
22. Y. Xu and J. Xiao, Sci. Rep. UK **6**, 27949 (2016).
23. X. Chen, C. Qiu, Z. Sheng, A. Wu, H. Huang, Y. Zhao, W. Li, X. Wang, S. Zou, and F. Gan, Chin. Opt. Lett. **14**, 081301 (2016).
24. Y. Xiong, D. Xu, J. H. Schmid, P. Cheben, S. Janz, and W. N. Ye, Opt. Express **22**, 17458 (2014).
25. Y. Ding, L. Liu, C. Peucheret, and H. Ou, Opt. Express **20**, 20021 (2012).
26. D. K. Gramotnev and S. I. Bozhevolnyi, Nat. Photonics **4**, 83 (2010).
27. D. Dai and S. He, Opt. Express **17**, 16646 (2009).
28. S. K. Selvaraja, W. Bogaerts, P. Dumon, D. V. Thourhout, and R. Baets, IEEE J. Sel. Top. Quantum Electron. **16**, 316 (2010).
29. D. Dai and J. E. Bowers, Opt. Express **19**, 18614 (2011).
30. H. A. Haus and W. Huang, Proc. IEEE **79**, 1505 (1991).
31. M. Z. Alam, J. S. Aitchison, and M. Mojahedi, IEEE J. Sel. Top. Quant. **19**, 4602008 (2013).
32. H. Deng, D. O. Yevick, C. Brooks, and P. E. Jessop, J. Lightwave Technol. **23**, 432 (2005).
33. L. Gao, L. Tang, F. Hu, R. Guo, X. Wang, and Z. Zhou, Opt. Express **20**, 11487 (2012).